The contribution of hippocampal subfields to the progression of neurodegeneration

Kichang Kwak[1], Marc Niethammer[1,2], Kelly S. Giovanello[1,3], Martin Styner[2,4], Eran Dayan[1,5*] for the

Alzheimer's Disease Neuroimaging Initiative[†]

1. Biomedical Research Imaging Center, University of North Carolina at Chapel Hill

2. Department of Computer Science, University of North Carolina at Chapel Hill

3. Department of Psychology and Neuroscience, University of North Carolina at Chapel Hill

4. Department of Psychiatry, University of North Carolina at Chapel Hill

5. Department of Radiology, University of North Carolina at Chapel Hill

* *Corresponding author*

Eran Dayan, Ph.D.

Email: eran_dayan@med.unc.edu

Abstract

Mild cognitive impairment (MCI) is often considered the precursor of Alzheimer's disease. However, MCI is associated with substantially variable progression rates, which are not well understood. Attempts to identify the mechanisms that underlie MCI progression have often focused on the hippocampus, but have mostly overlooked its intricate structure and subdivisions. Here, we utilized deep learning to delineate the contribution of hippocampal subfields to MCI progression. We propose a dense convolutional neural network architecture that differentiates stable and progressive MCI based on hippocampal morphometry with an accuracy of 75.85%. A novel implementation of occlusion analysis revealed marked differences in the contribution of hippocampal subfields to the performance of the model, with presubiculum, CA1, and subiculum showing the most central role. Moreover, the analysis reveals that more than 20% of the hippocampal volume was redundant in the differentiation between stable and progressive MCI.

Introduction

A certain degree of cognitive decline is common and considered a part of the normal aging process. Mild cognitive impairment (MCI) occurs when cognitive decline exceeds what is expected given an individual's age and education level (*1*). MCI can be considered a transitional phase in between age-related cognitive decline and Alzheimer's disease (AD) or other dementias (*1*). However, MCI is associated with marked etiological heterogeneity (*2*) and variable progression rates (*3*). Namely, up to 33% of individuals with MCI convert to AD over 5 years (*4*), with annual conversion rates of about 7% (*5*), but others may remain stable or even revert to normal or near-normal cognition levels (*6*). Identifying prognostic markers that can predict eventual conversion from MCI to AD is of profound clinical interest (*7*). However, such markers are not available to date. Fundamentally, despite increased interest in recent years (*8–10*), a mechanistic framework for understanding progression and stability in MCI remains missing.

The neuropathological profile of MCI is complex and multifaceted (*11*). As MCI is commonly seen as a precursor to AD, many studies have focused on alterations in structures known to be affected by this disease. The most widely studied target in AD is the hippocampus (*12*, *13*) , and indeed, multiple studies have reported hippocampal volume loss in MCI relative to controls (*14*). Studies have also implicated the hippocampus in the progression of MCI (*15*). Of particular interest, a series of recent studies have utilized deep learning to differentiate progressive and stable MCI (*16*, *17*) or predict individual subjects' progression from MCI to AD (*18*) based on whole hippocampus structural features. However, rather than being a homogeneous structure, the hippocampus is complex and heterogeneous (*19*). The hippocampus is composed of several histologically distinct subfields (*19*), which are characterized by differential connectivity profiles (*20*) and subserve different memory processes (*21*). Thus, a better understanding of MCI progression and stability necessitates a mechanistic framework that takes the structural complexity of the hippocampus into account (*22*). The literature, nevertheless, presents mixed and inconsistent findings in regards to the contribution of hippocampal subfields to MCI progression and stability (*23*, *24*).

3

In the current study, we investigated the contribution of hippocampal subfields to the progression and stability of MCI utilizing a deep learning framework and a large neuroimaging dataset. We propose a deep convolutional neural network trained to classify stable and progressive MCI based on hippocampal structural features derived from magnetic resonance imaging (MRI). We then introduce a novel implementation of occlusion analysis to prospectively evaluate the relative contribution of each hippocampal subfield to the performance of the predictive model. Moreover, the same analysis allowed us to estimate the cumulative contribution of subfields to MCI stability and the possible existence of redundancy within the associated hippocampal features.

Results

To delineate the contribution of hippocampal subfields to MCI progression we analyzed neuroimaging data from the Alzheimer's Disease Neuroimaging Initiative (ADNI). Our analysis focused on individuals with MCI who exhibit progressive deterioration in cognitive performance in comparison to those who remain stable over time (Fig. 1A). We thus considered data from two groups (Fig 1B). First, subjects in the stable MCI (sMCI) group had a baseline diagnosis of MCI which was retained at follow-up, with at least 18 months between diagnoses. Secondly, subjects in the progressive MCI (pMCI) were subjects who over the course of a similar duration progressed from a diagnosis of MCI to AD. To train our deep learning model (see below) we additionally analyzed data from cognitively normal (CN) subjects along with subjects with a diagnosis of AD. Two independent cohorts were analyzed for the two latter groups (data from ADNI-1 and ADNI-2/GO).

-- Figure 1 Here--

Participant Characteristics

The demographic characteristics of subjects in the AD, CN, pMCI and sMCI groups are shown in **Table 1**. Comparing the pMCI and sMCI groups, there were significant differences in age ($t_{379} = 2.449$, $p = 0.015$) and MMSE score (Wilcoxon Rank-sum, $Z = 4.938$, $p = 7.89 \times 10^{-7}$). No significant difference was observed for gender distribution ($\chi^2 = 0.072$, $p = 0.787$) or education ($t_{379} = 0.756$, $p =$

0.450). In the comparisons between the AD and CN groups, in both cohorts there were significant differences in education (ADNI -1: $t_{425} = 4.483$, $p = 9.47 \times 10^{-6}$; ADNI-2/GO: $t_{347} = 2.614$, $p = 0.009$) and MMSE score (ADNI-1: $Z = 17.900$, $p = 1.19 \times 10^{-71}$; ADNI-2/GO: $Z = 15.953$, $p = 2.70 \times 10^{-57}$). Age significantly differed in the ADNI-2/GO ($t_{347} = 1.901$, $p = 0.058$) cohort, but not in ADNI-1($t_{425} = 0.562$, $p = 0.575$). Gender distributions were not significantly different in both cohorts (ADNI-1: $\chi^2 = 0.022$ $p = 0.882$; ADNI-2/GO: $\chi^2 = 3.374$, $p = 0.066$).

Table 1 Demographics

	ADNI-1		ADNI-2 & GO			
	AD	CN	AD	CN	pMCI	sMCI
N	197	230	159	190	118	263
Age	75.6 ± 7.7	76.0 ± 5.0	74.8 ± 8.1	73.4 ± 6.4	73.6 ± 7.1	71.7 ± 7.3
Gender, female	95 (48.2%)	112 (48.7%)	68 (42.8%)	100 (52.6%)	52 (44.1%)	112 (42.6%)
Education	14.7 ± 3.1	16.0 ± 2.8	15.8 ± 2.7	16.5 ± 2.6	16.0 ± 2.7	16.2 ± 2.7
MMSE	23.3 ± 2.0	29.1 ± 1.0	23.1 ± 2.1	29.0 ± 1.3	27.3 ± 1.8	28.3 ± 1.7

Continuous variables are presented as mean ± SD and categorical variable is presented as %. Abbreviations: AD = Alzheimer's Disease, CN = Cognitively normal, pMCI = progressive mild cognitive impairment, sMCI = stable mild cognitive impairment, N = number of subjects, MMSE = Mini-Mental State Examination.

A deep learning model for classifying stable and progressive MCI

We next developed a deep learning model (Fig. 1C) for classification of pMCI vs. sMCI, as an initial step prior to delineating the role of hippocampal subfields in MCI progression. The inputs of the proposed model were hippocampal intensity values derived from subjects' structural MRI. Inputs were derived from a 3D bounding box obtained by cropping around the left and right hippocampus. The size of the 3D bounding box for each hippocampus was 44 x 52 x 52 voxels. As in previous studies (*16*, *18*) the deep learning model was trained to first differentiate the AD and CN groups and then tested on the task of differentiating the pMCI and sMCI groups. Data augmentation was applied within the training data set to improve the performance of the model and its generalizability. We randomly divided the training data set into 10 folds and 10-fold cross-validation was used within the training set to optimize and fine-tune the model's parameters. The model with the best performance achieved maximal accuracy of 94.07% in one of the folds, with an area under the curve (AUC) of the

receiver operating characteristic (ROC) of 0.993. The model was further validated with AD and CN data from ADNI-1, achieving an accuracy of 86.20%, with an AUC of 0.937 (Fig 2A). Thus, despite a decrease in accuracy, which may be expected given that ADNI-1 is based on lower MRI field strength (1.5T, relative to ADNI 2/GO's 3T) the model was overall stable and robust. This model was thus used next for differentiating the pMCI and sMCI groups based on data from ADNI-2/GO. In this task, the model achieved an accuracy of 75.85% and an AUC of 0.777 (Fig. 2B). Repeating the analysis with an age-matched test cohort had minimal effects on the accuracy of the model (fig. S1).

Overall our proposed deep learning-based classification framework corroborates earlier results, by demonstrating comparable accuracy performance to those reported previously for the classification of pMCI vs. sMCI (*16–18*). It demonstrates that whole-hippocampus structural features can be used to differentiate pMCI from sMCI.

-- Figure 2 Here--

Contribution of hippocampal subfields to MCI progression: occlusion analysis

We next sought to test if differentiation of pMCI from sMCI can be achieved with data derived from single hippocampal subfields, assessing the relative contribution of each subfield to classification performance. We first segmented the hippocampal subfields in each of the subjects using a validated automated method (*25*) (Fig. 3A). The contribution of each subfield was then assessed using an adaption of occlusion analysis, a common approach in computer vision (e.g., (*26*)). Briefly, in this analysis we retested the deep learning model, each time occluding a binary mask of each of the hippocampal subfields from the model's test data (i.e., from the 3D bounding box). The occlusion was achieved by setting the intensity values of each hippocampal subfield to zero in the input data. The performance (accuracy) of the models were then ranked and compared to each other as well as to the model based on an intact hippocampus (Fig. 3B). Accuracy levels for each of the models differed considerably (Fig. 3C)**.** Except for the molecular layer, the occlusion of subfields led to a decrease in accuracy. In particular, occlusion of the subiculum, CA1, and presubiculum led to dramatic decreases in accuracy, relative to other subfields, including CA2/3 and CA4 for example. Thus, the presubiculum, subiculum, and CA1 had the largest impact on the performance of the model (Fig. 3D).

6

-- Figure 3 Here--

The occlusion analysis revealed that many of the subfields had little to no contribution to the performance of the model. Namely, occlusion of CA2/3 and parasubiculum, for example, resulted in an accuracy loss of less than 5%. This suggests that in the classification of pMCI and sMCI some of the subfields may be redundant. We evaluated this possibility by performing a sequential version of the occlusion analysis, where occlusion is accumulated from step to step (Fig.4A), in descending order with respect to each subfield's contribution to the model's performance (as reported in Fig. 3). Accuracy was evaluated as a function of the ratio of the total occluded volume to the volume of the entire hippocampus. In comparison to the model with no occlusion, the accuracy started decreasing when 20.1% of the volume of the hippocampus was removed (with occlusion of the molecular layer, fimbria, parasubiculum, CA2/3, and HATA). In other words, we found that more than 20 % of the volume of the hippocampus was redundant in classifying pMCI versus sMCI. Upon removal of more than 78.5% of the volume of the hippocampus accuracy levels started saturating.

-- Figure 4 Here--

Discussion

Individuals with MCI show strongly variable symptomatic trajectories, with some progressing eventually to a probable diagnosis of AD, while others showing a more stable pattern of cognitive performance over time. In this paper, we propose a novel framework for the analysis of the progression and stability in of MCI based on deep learning and occlusion analysis. First, we introduced a deep convolutional neural network model based on the DenseNet architecture (*27*) for classifying pMCI vs. sMCI. Second, we proposed a novel analytical framework based on occlusion analysis to evaluate the contribution of hippocampal subfields on the performance of the proposed deep learning model, thus assessing the role of the different subfields in the stability and progression of MCI. Finally, as a secondary step, we applied a gradually accumulating occlusion analysis which allowed us to assess the degree of redundancy in the hippocampal features in relation to the classification of pMCI and sMCI.

7

As an initial step prior to the evaluation of the role of hippocampal subfields, we trained a deep convolutional neural network to classify the pMCI and sMCI groups based on all structural hippocampus features. This model achieved an accuracy of 75.85% (and an AUC of 0.777). This classification performance in on par with earlier deep learning models developed to classify pMCI vs. sMCI based on whole hippocampus structural features or multi-model features (e.g., (*28*, *29*)), which ranged from 72% to 76%. For example, a 3D-convolutional neural network based on multi-modal data, integrating structural MRI and positron emission tomography classified pMCI vs. sMCI with an accuracy of 72.22% (*16*), while another recently described a hybrid convolutional and recurrent neural network based on internal and external hippocampal patches yielded classification accuracy of 72.50% for the same task (*17*). Another recent study utilized deep learning and hippocampal features predicting progression time from MCI to AD with a concordance index of 0.762 (*18*). Our model corroborates these earlier reports by demonstrating that prediction of MCI stability and progression can be achieved with good accuracy rates based solely on hippocampal features.

Our findings extend earlier reports by delineating the contribution of singe hippocampal subfields to the progression and stability of MCI. Our implementation of occlusion analysis revealed marked differences between the subfields in differentiating the pMCI and sMCI groups. In particular, the results suggest that the subiculum, presubiculum, and CA1 were more central to this classification task than any other subfield. The findings are consistent with earlier reports on the involvement of CA1 and the subiculum in the progression of MCI (*30*, *31*). While several studies implicated CA2/3, fimbria, and GC-DG in MCI progression (*23*, *24*), our model suggests that these subfields play a more minor role. Our findings may reflect the neuropathological cascade characteristic of AD. Namely, neurofibrillary tangles in AD neurodegeneration progress from CA1 to the subiculum, before reaching CA2/3 (*32*), Neuronal loss in CA1 is prominent as AD neurodegeneration progresses, while being milder and slower in the subiculum (*33*). Although our findings highlight the contribution of subiculum, presubiculum, and CA1 in the progression of MCI further examination into the possible involvement of other subfields is warranted.

8

As a secondary step to the occlusion analysis, which helped us evaluate the contribution of single subfields to MCI progression and stability, we also evaluated how accumulated occlusion of hippocampal features affected the results. This analysis revealed that more than 20% of the volume of the hippocampus was redundant in the differentiation between pMCI and sMCI. These results may reflect the progressive nature of neurodegeneration in AD, wherein the redundant subfields have yet to have been affected, and thus do not yet differentiate among patients with stable and progressive progression trajectories. Another speculative possibility, which remains to be tested in future research is that the redundancy reflects neuroprotective mechanisms that allow individuals with MCI to compensate for the earlier phases of neurodegeneration. Compensatory and reserve mechanisms have been widely postulated to operate in response to aging and neurodegeneration (*34*, *35*). Future research could test if redundancy at the level of hippocampal structure is functionally advantageous, offering patients with a coping mechanism for early-phase neurodegeneration.

Several limitations should be noted. First, while our study considered longitudinal clinical evaluations we did not examine longitudinal changes in imaging metrics. Our focus here was on evaluations of prognostic markers of conversion from MCI to AD. Future research could use similar methods to examine longitudinal imaging data. Second, we considered a single imaging modality in our models (structural MRI). Studies have consistently revealed the superiority of multimodal features in diagnostic and prognostic models (e.g., (*28*)). Since our focus here was on hippocampal subfields, integration of data with lower spatial resolution like that obtained from PET Amyloid Imaging would have been challenging. Yet, we acknowledge that basing our models on a single modality may have reduced its performance in the classification task. Finally, it would be beneficial to replicate the results with data obtained with higher-resolution neuroimaging.

In conclusion, the current study delineates the contribution of hippocampal subfields to the progression and stability of MCI, highlighting the central role of the subiculum, presubiculum, and CA1 in differentiation between pMCI and sMCI. The results further reveal that more than 20% of the volume of the hippocampus is redundant in the differentiation between these two groups. These

results highlight the need to consider the intricate structure of the hippocampus in studies of AD neurodegeneration.

Materials and Methods

Experimental data

Data used in the preparation of this article were obtained from the ADNI database (adni.loni.usc.edu). The ADNI was launched in 2003 as a public-private partnership, led by Principal Investigator Michael W. Weiner, MD. The primary goal of ADNI has been to test whether serial magnetic resonance imaging (MRI), other biological markers, and clinical and neuropsychological assessment can be combined to measure the progression of MCI and early AD. For up-to-date information, see www.adni-info.org. All subjects provided written informed consent and the study protocol was approved by the local Institutional Review Boards. We used data from 349 subjects from ADNI-2/GO to train the deep learning model and evaluated the model with an independent cohort of 427 subjects from ADNI-1. An additional sample of 381 subjects with MCI at baseline, obtained from ADNI-2/GO, was classified as either sMCI or pMCI based on longitudinal diagnostic evaluations. We excluded subjects who were diagnosed with MCI at baseline but reverted to CN during follow-up. The demographic characteristics of each cohort analyzed in this study are summarized in Table 1.

Imaging data

Input data for the deep learning model were acquired at ADNI sites using 1.5T (ADNI1) and 3T (ADNI-2/GO) scanners and were based on either an inversion recovery-fast spoiled gradient recalled (IR-SPGR) or a magnetization-prepared rapid gradient-echo (MP-RAGE) sequences (*36*). Full details of the image acquisition parameters are listed on the ADNI website (http://adni.loni.usc.edu/methods/documents/mri-protocols/).

Image Processing

Input data from the left and right hippocampus were extracted from the T1-weighted MRI images. We first defined a 3D bounding box of size $44 \times 52 \times 52$ voxels around the hippocampal region. The size of the bounding box ensured coverage of the entire hippocampus across the entire sample of subjects.

Intensity values from each voxel within the bounding box were then extracted and used as inputs in the deep learning model described below.

Data Augmentation: To artificially increase the size of the model's training dataset, and improve its performance and generalizability, we used an image data augmentation technique with Scikit-learn 0.22.1 (*37*). The augmented image data were generated through the addition of noise with mean 0 and standard deviation 1, contrast enhancement by effectively spreading out the most frequent intensity values (stretching out the intensity range) and flipping left and right. In total, 954 AD images, and 1140 CN images were generated through augmentation and used in the training dataset to improve the performance of the model.

Hippocampal subfield segmentation: Subfields in the hippocampus were segmented with an automated segmentation tool available in FreeSurfer v6.0 (*38*), which is based on a new statistical atlas built primarily upon ultra-high resolution (~0.1mm isotropic), *ex vivo* MRI data. This approach uses Bayesian inference that relied on image intensities and a tetrahedral mesh-based probabilistic atlas of the hippocampal formation, constructed from a library of *in vivo* data and *ex vivo* labeled data (*38, 39*). The left and right hippocampus were segmented into twelve subfields: CA1, CA2/3, CA4, hippocamps-amygdala transition area (HATA), granule cell layer of the dentate gyrus (GC-DG), fimbria, molecular layer, hippocampal fissure, hippocampal tail, subiculum, parasubiculum and subiculum.

Deep learning model architecture

A deep learning model based on the DenseNet architecture (*27*) was trained to learn relevant maps for classifying pMCI vs. sMCI. The deep learning model (See Fig. 1C) was comprised of two streams for the left and right hippocampus. Each stream consisted of a convolutional layer, 4 dense blocks, 3 transition layers, and a global average pooling layer. The outputs of the two streams were then concatenated as input to a fully connected layer. First, the image was passed through a stack of convolutional layers, where the filters were of size 5×5×5. The convolution stride was fixed to 1 voxel; The max-pooling layer had a stride of size 2×2×2 and a kernel size of 2×2×2. The dense block consisted of multiple convolution units, which were equipped with batch normalization layer,

11

leaky rectified linear unit, a 1×1×1 convolutional layer, a 3×3×3 convolutional layer and a dropout layer. Every convolutional unit was connected to all previous layers by shortcut connections. A transition layer allowed for dimensionality reduction of feature maps in between dense blocks. It was composed of a batch normalization layer, leaky rectified linear unit, a 1×1×1 convolutional layer, a 3×3×3 convolutional layer, a dropout layer and an averaging pooling layer. The stacks of global averaging pooling layers were concatenated and connected by a fully-connected layer. The output value is processed by the fully-connected layer with a sigmoid activation function.

Implementation

The deep learning model was built with the Keras application programming interface in Tensorflow 2.0. Training and testing of the model were carried out with an Ubuntu 18.04.3 operating system and two Nvidia Tesla V100 graphic cards with 16GB memory each. The model was parallelized across graphic cards. We trained the model with a mini-batch size of 64 and 200 epochs. The deep learning model was optimized using stochastic gradient descent (*40*) with momentums and an exponentially decaying learning rate. The initial learning rate was 0.0001 and it was decayed by 0.9 after every 10000 steps. We added a dropout layer in the dense block and set the dropout rate to 0.2. In the batch normalization, beta and gamma weight were initialized with L2 regularization set at 1×10^{-4} and epsilon set to 1.1×10^{-5}. The L2 regularization penalty coefficient was set at 0.01 for the fully connected layer.

Validation framework

We evaluated the performance of the proposed deep learning model using k-fold cross-validation, which allowed for the optimization of hyperparameters in the train set. We thus split the entire ADNI-2/GO data into k folds, selecting the parameters with the best performance and then applied the selected parameter to test data to validate the performance of the proposed model.

Implementation of occlusion analysis

Occlusion analysis was used for investigating the contribution of each hippocampal subfield to the performance of the prediction model. Masks for each hippocampal subfield were generated based on

12

the subfield segmentation procedure described above (See Image Processing). We then masked out each hippocampal subfield (set voxels of each hippocampal subfield to zero) from the input data of the test phase and retested the trained deep learning model as described before. Each occluded hippocampal subfield was thus ranked based on the performance (accuracy) of the model, relative to the original model, where input data from the entire hippocampus was used.

In a second implementation of occlusion analysis, we evaluated the performance of the prediction model under gradually accumulating occlusion of hippocampal subfields. This was achieved by retesting the prediction model, each time masking out an additional subfield (i.e., starting from one masked out subfield, then two etc.). Subfields were masked out sequentially, in descending order, according to their contribution to accuracy (as identified in the initial occlusion analysis). This step also allowed us to evaluate the stability of the occlusion analysis, ensuring that did not result in abrupt changes in classification performance.

References

1. S. Gauthier, B. Reisberg, M. Zaudig, R. C. Petersen, K. Ritchie, K. Broich, S. Belleville, H. Brodaty, D. Bennett, H. Chertkow, J. L. Cummings, M. de Leon, H. Feldman, M. Ganguli, H. Hampel, P. Scheltens, M. C. Tierney, P. Whitehouse, B. Winblad, Mild cognitive impairment. *Lancet*. **367**, 1262–1270 (2006).

2. C. DeCarli, Mild cognitive impairment: Prevalence, prognosis, aetiology, and treatment. *Lancet Neurol.* **2**, 15–21 (2003).

3. R. Roberts, D. S. Knopman, Classification and epidemiology of MCI. *Clin. Geriatr. Med.* **29**, 753–772 (2013).

4. A. Ward, S. Tardiff, C. Dye, H. M. Arrighi, Rate of Conversion from Prodromal Alzheimer's Disease to Alzheimer's Dementia: A Systematic Review of the Literature. *Dement. Geriatr. Cogn. Dis. Extra*. **3**, 320–332 (2013).

5. A. J. Mitchell, M. Shiri-Feshki, Rate of progression of mild cognitive impairment to dementia - Meta-analysis of 41 robust inception cohort studies. *Acta Psychiatr. Scand.* **119**, 252–265 (2009).

6. T. D. Koepsell, S. E. Monsell, Reversion from mild cognitive impairment to normal or near-Normal cognition; Risk factors and prognosis. *Neurology*. **79**, 1591–1598 (2012).

7. T. Karakaya, F. Fußer, J. Schröder, J. Pantel, Pharmacological Treatment of Mild Cognitive Impairment as a Prodromal Syndrome of Alzheimer´s Disease. *Curr. Neuropharmacol.* **11**, 102–108 (2013).

8. B. Cheng, M. Liu, D. Zhang, D. Shen, Robust multi-label transfer feature learning for early diagnosis of Alzheimer's disease. *Brain Imaging Behav.* **13**, 138–153 (2019).

9. M. Liu, J. Zhang, E. Adeli, D. Shen, Landmark-based deep multi-instance learning for brain disease diagnosis. *Med. Image Anal.* **43**, 157–168 (2018).

10. K. H. Thung, C. Y. Wee, P. T. Yap, D. Shen, Identification of progressive mild cognitive impairment patients using incomplete longitudinal MRI scans. *Brain Struct. Funct.* **221**, 3979–3995 (2016).

11. B. C. M. Stephan, S. Hunter, D. Harris, D. J. Llewellyn, M. Siervo, F. E. Matthews, C. Brayne, The neuropathological profile of mild cognitive impairment (MCI): A systematic review. *Mol. Psychiatry*. **17**, 1056–1076 (2012).

12. C. R. Jack, R. C. Petersen, P. C. O'Brien, E. G. Tangalos, MR-based hippocampal volumetry in the diagnosis of Alzheimer's disease. *Neurology*. **42**, 183–183 (1992).

13. N. C. Fox, E. K. Warrington, P. A. Freeborough, P. Hartikainen, A. M. Kennedy, J. M. Stevens, M. N. Rossor, Presymptomatic hippocampal atrophy in Alzheimer's disease. *Brain*. **119**, 2001–2007 (1996).

14. C. R. Jack, R. C. Petersen, Y. C. Xu, P. C. O'Brien, G. E. Smith, R. J. Ivnik, B. F. Boeve, S. C. Waring, E. G. Tangalos, E. Kokmen, Prediction of AD with MRI-based hippocampal volume in mild cognitive impairment. *Neurology*. **52**, 1397–1397 (1999).

15. G. Douaud, R. A. L. Menke, A. Gass, A. U. Monsch, A. Rao, B. Whitcher, G. Zamboni, P. M. Matthews, M. Sollberger, S. Smith, Brain Microstructure Reveals Early Abnormalities more than Two Years prior to Clinical Progression from Mild Cognitive Impairment to Alzheimer's Disease. *J. Neurosci.* **33**, 2147–2155 (2013).

16. Y. Huang, J. Xu, Y. Zhou, T. Tong, X. Zhuang, Diagnosis of Alzheimer's disease via multi-modality 3D convolutional neural network. *Front. Neurosci.* **13** (2019), doi:10.3389/fnins.2019.00509.

17.   F. Li, M. Liu, A hybrid Convolutional and Recurrent Neural Network for Hippocampus Analysis in Alzheimer's Disease. *J. Neurosci. Methods*. **323**, 108–118 (2019).

18.   H. Li, M. Habes, D. A. Wolk, Y. Fan, A deep learning model for early prediction of Alzheimer ' s disease dementia based on hippocampal magnetic resonance imaging data. *Alzheimer's Dement*. **15**, 1059–1070 (2019).

19.   H. M. Duvernoy, F. Cattin, P. Y. Risold, J. L. Vannson, M. Gaudron, *The human hippocampus: Functional anatomy, vascularization and serial sections with MRI, fourth edition* (Springer Berlin Heidelberg, 2013).

20.   M. A. Dalton, C. McCormick, E. A. Maguire, Differences in functional connectivity along the anterior-posterior axis of human hippocampal subfields. *Neuroimage*. **192**, 38–51 (2019).

21.   T. Bartsch, J. Döhring, A. Rohr, O. Jansen, G. Deuschl, CA1 neurons in the human hippocampus are critical for autobiographical memory, mental time travel, and autonoetic consciousness. *Proc. Natl. Acad. Sci. U. S. A.* **108**, 17562–17567 (2011).

22.   A. Maruszak, S. Thuret, Why looking at the whole hippocampus is not enough-a critical role for anteroposterior axis, subfield and activation analyses to enhance predictive value of hippocampal changes for Alzheimer's disease diagnosis. *Front. Cell. Neurosci.* **8**, 1–11 (2014).

23.   Y.-D. Li, H.-B. Dong, G.-M. Xie, L. Zhang, Discriminative Analysis of Mild Alzheimer's Disease and Normal Aging Using Volume of Hippocampal Subfields and Hippocampal Mean Diffusivity. *Am. J. Alzheimer's Dis. Other Dementiasr*. **28**, 627–633 (2013).

24.   W. Khan, E. Westman, N. Jones, L. O. Wahlund, P. Mecocci, B. Vellas, M. Tsolaki, I. Kłoszewska, H. Soininen, C. Spenger, S. Lovestone, J. S. Muehlboeck, A. Simmons, Automated Hippocampal Subfield Measures as Predictors of Conversion from Mild Cognitive Impairment to Alzheimer's Disease in Two Independent Cohorts. *Brain Topogr.* **28**, 746–759 (2015).

25.   E. M. Brown, M. E. Pierce, D. C. Clark, B. R. Fischl, J. E. Iglesias, W. P. Milberg, R. E. McGlinchey, D. H. Salat, Test-retest reliability of FreeSurfer automated hippocampal subfield segmentation within and across scanners. *Neuroimage*. **210**, 116563 (2020).

26.   Suha Kwak, Woonhyun Nam, Bohyung Han, Joon Hee Han, in *2011 International Conference on Computer Vision* (IEEE, 2011; http://ieeexplore.ieee.org/document/6126414/), pp. 1551–1558.

27.   G. Huang, Z. Liu, L. Van der Maaten, K. Q. Weinberger, Densely Connected Convolutional Networks. *CVPR* (2017).

28.   H.-I. Suk, S.-W. Lee, D. Shen, Hierarchical feature representation and multimodal fusion with deep learning for AD/MCI diagnosis. *Neuroimage*. **101**, 569–582 (2014).

29.   R. Li, W. Zhang, H.-I. Suk, L. Wang, J. Li, D. Shen, S. Ji, Deep Learning Based Imaging Data Completion for Improved Brain Disease Diagnosis. *Med. Image Comput. Comput. Interv. – MICCAI 2014. Lect. Notes Comput. Sci.*, 305–312 (2014).

30.   G. A. Carlesimo, F. Piras, M. D. Orfei, M. Iorio, C. Caltagirone, G. Spalletta, Atrophy of presubiculum and subiculum is the earliest hippocampal anatomical marker of Alzheimer's disease. *Alzheimer's Dement. Diagnosis, Assess. Dis. Monit.* **1**, 24–32 (2015).

31.   L. G. Apostolova, R. A. Dutton, I. D. Dinov, K. M. Hayashi, A. W. Toga, J. L. Cummings, P. M. Thompson, Conversion of mild cognitive impairment to alzheimer disease predicted by hippocampal

atrophy maps. *Arch. Neurol.* **63**, 693–699 (2006).

32.   H. Braak, E. Braak, Neuropathological stageing of Alzheimer-related changes. *Acta Neuropathol.* **82** (1991), pp. 239–259.

33.   M. Rössler, R. Zarski, J. Bohl, T. G. Ohm, Stage-dependent and sector-specific neuronal loss in hippocampus during alzheimer's disease. *Acta Neuropathol.* **103**, 363–369 (2002).

34.   T. J. Montine, B. A. Cholerton, M. M. Corrada, S. D. Edland, M. E. Flanagan, L. S. Hemmy, C. H. Kawas, L. R. White, Concepts for brain aging: Resistance, resilience, reserve, and compensation. *Alzheimer's Res. Ther.* **11**, 10–12 (2019).

35.   R. Cabeza, M. Albert, S. Belleville, F. I. M. Craik, A. Duarte, C. L. Grady, U. Lindenberger, L. Nyberg, D. C. Park, P. A. Reuter-Lorenz, M. D. Rugg, J. Steffener, M. N. Rajah, Maintenance, reserve and compensation: the cognitive neuroscience of healthy ageing. *Nat. Rev. Neurosci.* **19**, 701–710 (2018).

36.   C. R. Jack, M. A. Bernstein, B. J. Borowski, J. L. Gunter, N. C. Fox, P. M. Thompson, N. Schuff, G. Krueger, R. J. Killiany, C. S. DeCarli, A. M. Dale, O. W. Carmichael, D. Tosun, M. W. Weiner, Update on the Magnetic Resonance Imaging core of the Alzheimer's Disease Neuroimaging Initiative. *Alzheimer's Dement.* **6**, 212–220 (2010).

37.   F. Pedregosa, G. Varoquaux, A. Gramfort, V. Michel, B. Thirion, Scikit-learn: Machine Learning in Python. *J. Mach. Learn. Res.* **12**, 2825–2830 (2011).

38.   J. E. Iglesias, J. C. Augustinack, K. Nguyen, C. M. Player, A. Player, M. Wright, N. Roy, M. P. Frosch, A. C. McKee, L. L. Wald, B. Fischl, K. Van Leemput, A computational atlas of the hippocampal formation using ex vivo, ultra-high resolution MRI: Application to adaptive segmentation of in vivo MRI. *Neuroimage*. **115**, 117–137 (2015).

39.   K. Van Leemput, A. Bakkour, T. Benner, G. Wiggins, L. L. Wald, J. Augustinack, B. C. Dickerson, P. Golland, B. Fischl, Automated segmentation of hippocampal subfields from ultra-high resolution in vivo MRI. *Hippocampus*. **19**, 549–557 (2009).

40.   D. P. Kingma, J. L. Ba, Adam: A method for stochastic optimization. *3rd Int. Conf. Learn. Represent.*, 1–15 (2015).

Acknowledgments

Author contribution: K.K and E.D conceived research; K.K. analyzed data; K.K, M.N, K.S.G, M.S and E.D interpreted results. K.K and E.D. wrote the paper.

Competing interest: The authors declare that they have no competing interests.

Data and materials availability: All data reported in the current study were obtained from the ADNI (http://adni.loni.usc.edu/). Other materials may be requested from the authors.
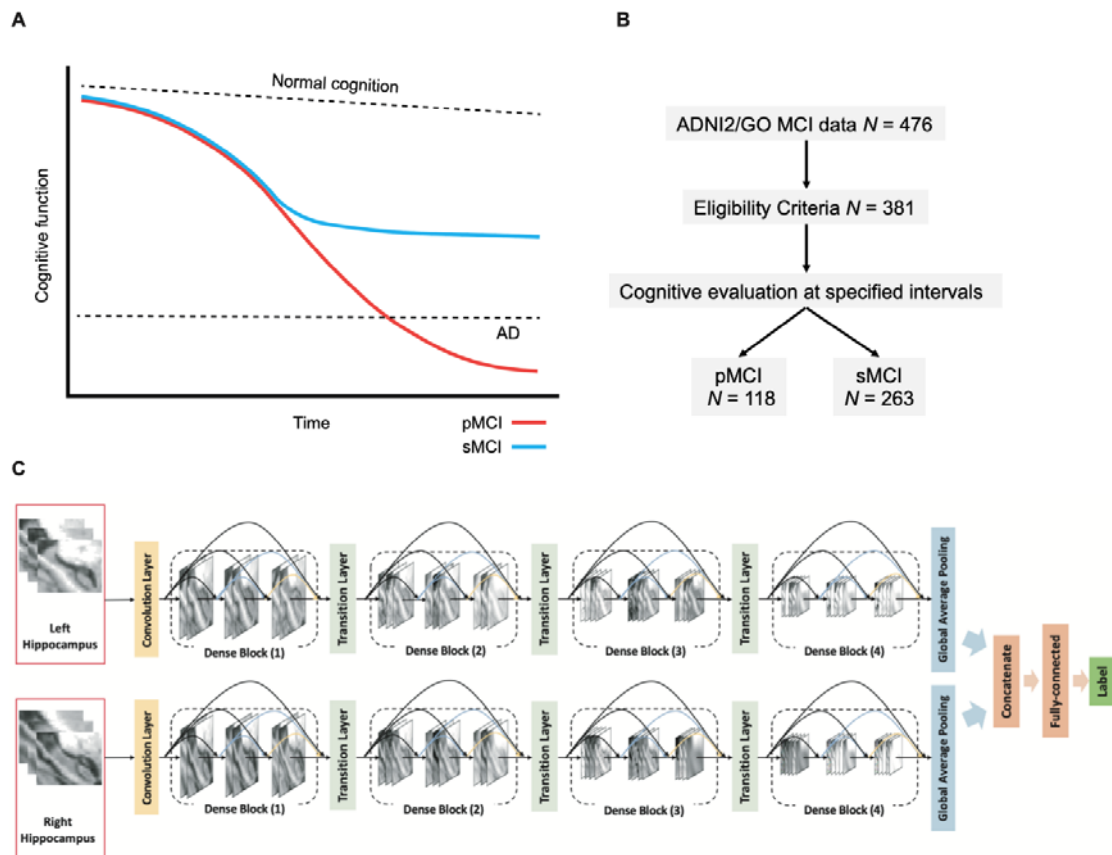
Figures:

Fig. 1. Study design and methods. (**A**) Hypothetical models of MCI progression. In pMCI gradual cognitive decline continues until individuals meet the diagnostic criteria of AD. In sMCI cognitive performance remains relatively stable over time. (**B**) Group allocation criteria. Cognitive evaluations at baseline and follow-up visits were used to classify subjects in the pMCI and sMCI groups. (**C**) Illustration of proposed deep learning model. Abbreviations: AD=Alzheimer's disease, MCI=mild cognitive impairment, pMCI=progressive mild cognitive impairment, sMCI=stable mild cognitive impairment.
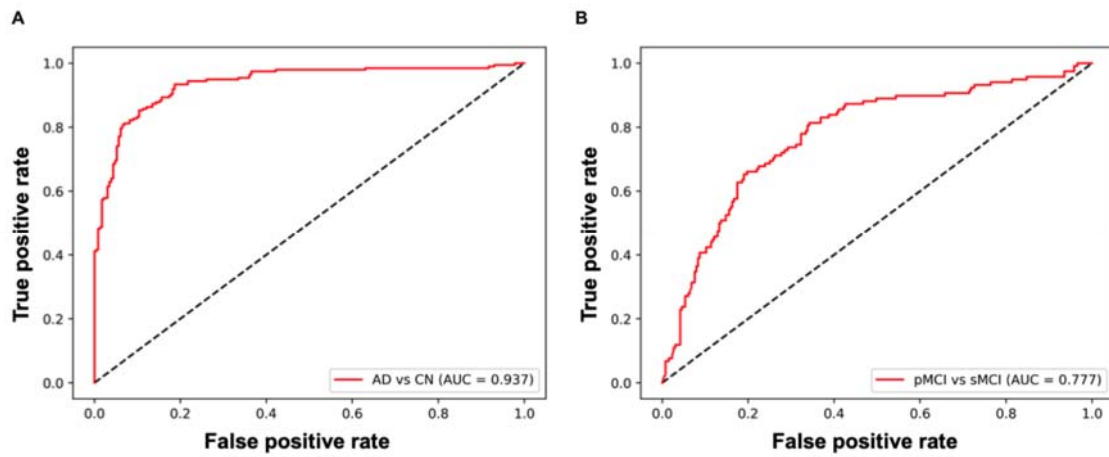
Fig. 2. ROC curves showing the performance of the proposed deep learning model. (A) For the AD versus CN task. **(B)** For the pMCI vs sMCI task. Abbreviations: AD=Alzheimer's disease, CN=cognitively normal, pMCI=progressive mild cognitive impairment, sMCI=stable mild cognitive impairment, ROC=receiver operating characteristic, AUC=area under the curve.
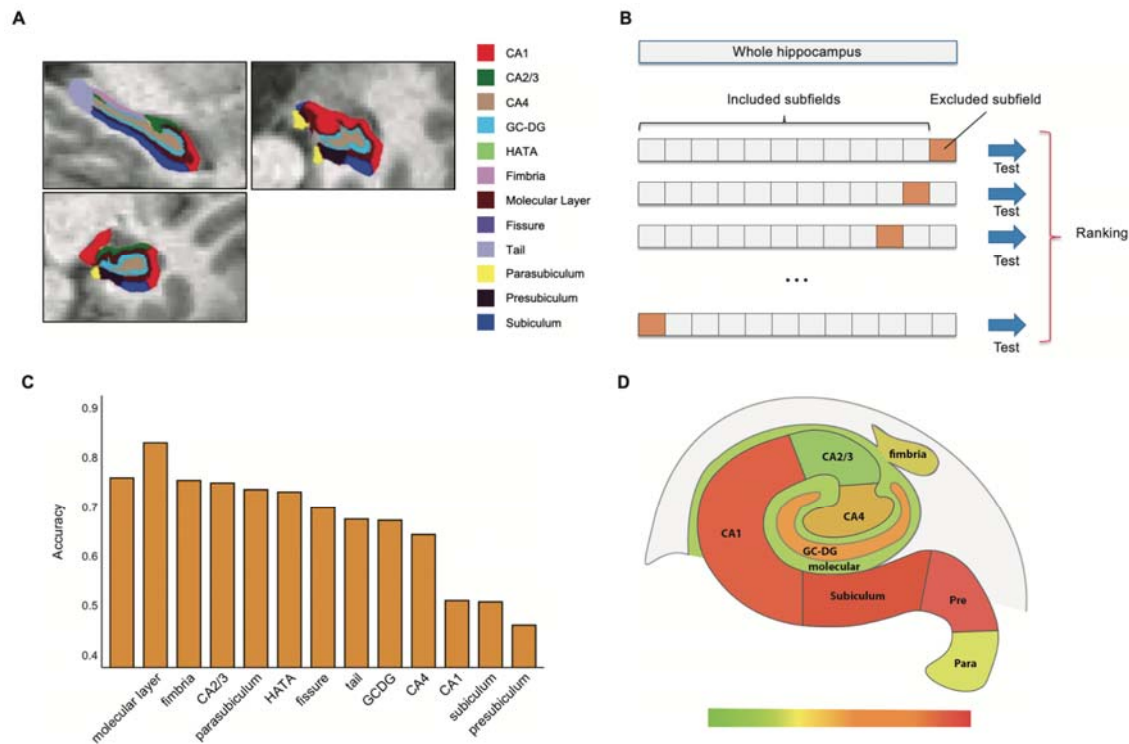
Fig. 3. Illustration of the occlusion analysis of hippocampal subfields. (A) Hippocampal subfield segmentation. The segmentation results of hippocampal subfields are illustrated on the single representative subject. **(B)** Schematic framework of the occlusion analysis. In each model, one of the hippocampal subfields was occluded (masked out) in the testing data and the performance of the model (its accuracy) was ranked relative to the occlusion of other subfields and to the performance of the original intact model. **(C)** The results of the occlusion analysis are shown for each model, along with the results of the original intact model **(D)** Accuracy performance of each model, superimposed on top of an illustration of the major hippocampal subfields (note: not all subfields are shown). Abbreviations: CA=cornu ammonis, HATA=hippocampus-amygdala-transition-area, GC-DG=granule cell layer of the dentate gyrus.
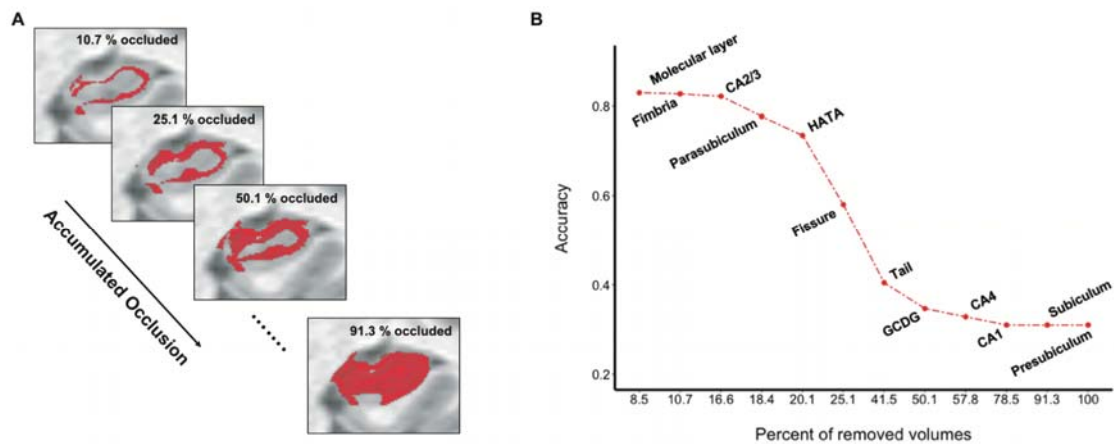
Fig. 4. Illustration of the accumulated occlusion analysis of hippocampal subfields. (A) An illustration of gradually accumulating occlusion. On each step, additional hippocampal volume is masked out of the analysis. **(B)** The model's accuracy is shown as a function of accumulated occlusion, with subfields masked out in descending order according to their contribution to the model's accuracy (as shown in Fig. 3C). The accuracy started decreasing (i.e., relative to the accuracy of the full model) upon removal of 20.1% of the volume of the hippocampus. Abbreviations: CA=cornu ammonis, HATA=hippocampus-amygdala-transition-area, GC-DG=granule cell layer of the dentate gyrus.